Peer-reviewed version available at *Metals* **2020**, *10*, 1177; doi:10.3390/met10091177

Article

Effect of inclusions on the corrosion properties of nickel based alloys 718 and EP718

Ekaterina Alekseeva [1], *, Andrey Karasev [2], *, Pär G. Jönsson [2] and Aleksey Alkhimenko [1]

[1] Peter the Great Saint-Petersburg Polytechnic University, Polytechnicheskaya 29, 194064, Saint-Petersburg, Russia;
[2] KTH Royal Institute of Technology, Brinellvägen 23, 100 44 Stockholm, Sweden;
* Correspondence: alekseeva_el@spbstu.ru; karasev@kth.se

Abstract: Inclusions in steels and alloys are known as factors that could lower deformation, mechanical, corrosion and other properties. Study of inclusions in nickel based alloys is important since these materials could suffer from corrosion degradation in harsh operational conditions, where inclusions could lead to a pitting initiation. For estimation of a harmful effect of different inclusions on corrosion resistance of Ni-based alloys, inclusion characteristics (such as composition, morphology, size, number and location) on film filter and dissolution of metal matrix around different inclusions on surfaces of metal samples after electrolytic extraction (EE) were investigated in two samples of industrial Ni-based alloys (alloy 718 and EP718). It was found that both Ni-based alloys have various inclusions: carbides (large size NbTi-C and small multicomponent carbides), nitrides TiNb-N and sulfides (TiNb-S in EP718 alloy). The higher harmful effect on corrosion resistance of metal was detected around sulfides and small carbides containing Mo, W, Cr. Dissolution effect was also observed around large carbides and nitrides, especially around inclusions having size more than 10 μm. Moreover, the dissolution of metal matrix around inclusions and clusters located on the grain boundaries is 2.1-2.7 times larger compared to that for those inclusions inside of grains of the given alloy samples.

Keywords: nickel based alloys; corrosion; inclusions, oil and gas industry, electrolytic extraction, alloy 718

1. Introduction

Many investigations show that inclusions (incoherent precipitates) that are formed during production [1, 2, 3] can significantly affect mechanical, corrosion, deformation, machining properties of steels and alloys that were shown for low alloyed steels and carbon steels [4, 5, 6], stainless steels [7, 8, 9, 10] and alloys [11, 12]. Main reasons of the effects concerned to voids or additionally stressed zones between matrix and inclusions that lead to the formation of microcracks and their propagation in a metal matrix. Another reason is that around inclusion are formed zones free or with lower concentrations of precipitated phases and elements contained in inclusions or metal zones depleted by alloying elements. As a result, the metal zones adjacent to inclusions are characterized by higher level of defects and higher stress [1]. Therefore, the mechanical properties and corrosion resistance of steels and alloys depend on the amount of these harmful inclusions, their size, morphology and distribution.

Ni-based alloys have a high corrosion resistance, mechanical properties and widely spread in industrial application as a material for wellhead component and downhole equipment for corrosive service at high temperatures and pressures in the presence of aggressive components (such as H_2S, CO_2, chlorides) [14]. Since Ni-based alloys have complicated chemistry, it leads to form of various deleterious inclusions and phases such as carbides, sulphides, delta-phase, etc. Some inclusions can initiate a pitting corrosion and could lead to environmentally assisted cracking, corrosion fatigue,

Peer-reviewed version available at Metals 2020, 10, 1177; doi:10.3390/met10091177

hydrogen embrittlement. Therefore, the study of corrosion and mechanical properties of Ni-based alloys and their dependence on different inclusions became the object of attention in many studies [15,16, 17, 18, 19, 20].

For instance, it was reported in [21, 22] that stable pittings started at Nb-C rich particles, whereas nitrides of Ti and Nb have a lower effect on corrosion [23]. Precipitation of carbides of chromium and tungsten (such as $M_{23}C_6$, M_6C) on the grain boundaries are also possible precursor sites for pitting in Ni-base alloys [24, 25]. Mo-rich phases are also a reason of sensitization and poor corrosion properties on the grain boundaries [26]. In [27] it was shown, that delta phase has a detrimental effect on passivation and potential breakdown of alloys. Moreover, delta phase is also a trapping site for hydrogen, which lowered resistance to hydrogen embrittlement and dependent upon the morphology of second phase particles [28, 29]. Despite of high velocity of crystallization additive technologies also give specific inclusion, so in [30, 31] it was founded coarse carbides of Ti, Nb, Cr, Mo, Nb/Mo-rich particles.

Thus, the Ni-based alloys contain various inclusions. However, at the moment there are unclear and contradictory data on the influence of composition, size, location and morphology of different inclusions on the corrosion properties. Therefore, the main goals of the present study are to test an application of electrolytic extraction for precise three-dimensional investigations of different inclusions and clusters (their composition, morphology, size, number and location in metal matrix) in two industrial Ni-based 718 and EP718 alloys and to evaluate the effect of various inclusions and clusters on corrosion resistance of these alloys by investigation of dissolution metal matrix around typical inclusions during electrolytic extraction process.

2. Materials and Methods

In order to investigate the effect of inclusions on corrosion properties two commercially available nickel based alloys were studied. The materials were produced by VIM+VAR processes, then forged and heat treated according corresponding specifications. The chemical composition of the studied materials is given in

Table 1. Chemical composition (% wt.) of the studied nickel based alloys

Alloy	C, max	Ni	Cr	Mo	Nb	Ti	W	Al	Fe	P, max	S, max
EP718	0.1	43-47	14-16	4.0-5.2	0.8-1.5	1.8-2.4	2.5-3.5	0.9-1.4	Bal.	0.01	0.015
Alloy 718	0.045	50-55	17-21	2.8-3.3	4.8-5.2	0.8-1.15		0.4-0.6	Bal.	0.01	0.01

Method of electrolytic extraction (EE) was used for 3D investigation of inclusions. Extraction was done in 10%AA electrolyte (10% acetylacetone – 1% tetramethyl-ammonium chloride-methanol) at the following parameters: electric current 0.04-0.06 A and voltage 2.9-3.8 V According to previous studies [32], this electrolyte for extraction was selected so as not to dissolve the detected inclusions during intensive dissolution of metal matrix. Therefore, it can be assumed that the inclusions were not directly involved in the electrochemical dissolution of the metal matrix around the inclusion. 0.08-0.10 g of alloy samples were dissolved during each electrolytic extraction, which correspond to a dissolved metal layer of 70-95 μm. After dissolution, the inclusions were collected on a surface of the polycarbonate film filter having a hole diameter of 0.4 μm.

Characteristics of non-metallic inclusions (such as composition, morphology, size, number and location) were analyzed by means of scanning electron microscopy (SEM) equipped with energy dispersive spectroscopy (EDS). The inclusions were investigated on a surface of film filters (FF) as

Peer-reviewed version available at Metals 2020, 10, 1177; doi:10.3390/met10091177

well on a surface of metal samples (MS) that were subjected to dissolution. The SEM images of typical inclusions investigated on a film filter and metal surface after EE are shown in Figure 1.

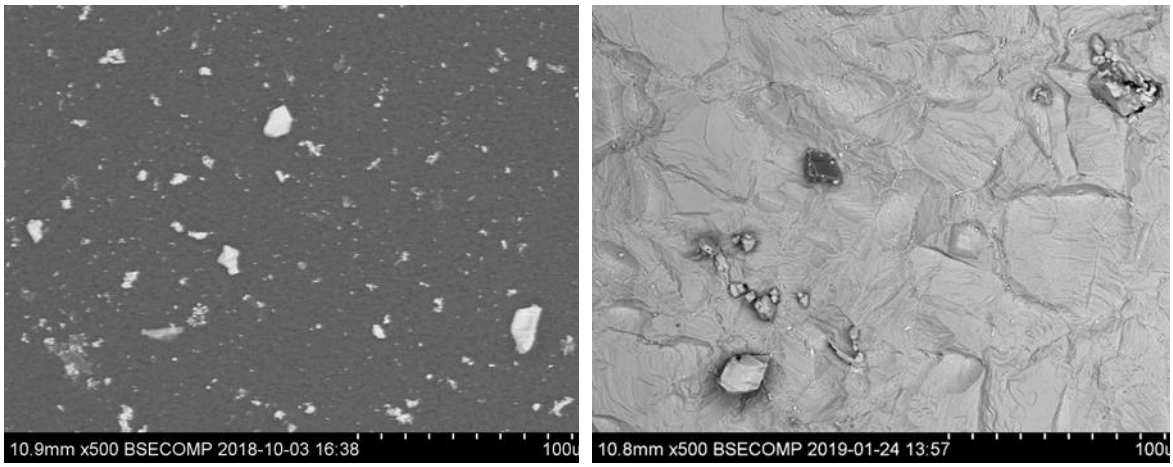

(a) **(b)**

Figure 1. Typical non-metallic inclusions investigated on film filter **(a)** and metal surface **(b)** after EE

For evaluation of the effect of inclusions on the corrosion resistance of alloy, a dissolution extent of metal matrix around different inclusions after electrolytic extraction was determined by measurement of diameters of the crater (D_{cr}) around inclusion and calculation of relative coefficient of metal dissolution (KD), which can be calculated as follows:

$$Dcr = \sqrt{(4 \times Acr/\pi)} \quad (1)$$

$$KD = A_{cr} / A_{incl} \quad (2)$$

where A_{cr} and A_{incl} are the area of the crater around an inclusion and the area of this inclusion measured on an SEM image, respectively.

3. Results

3.1. Characterization of inclusions after electrolytic extraction of metal samples

Based on the 3D investigations of inclusions on film filter and on the surface of metal samples after electrolytic extractions, it was found that the total number of inclusions per unit volume in EP718 is about 6.5 times larger than that in 718 alloy. However, in most cases, a determination only of the total content of all inclusions cannot explain the difference in corrosion resistance of similar steels or alloys. It is well known that different inclusions (having various characteristics such as compositions, morphology, size and location in metal matrix) can significantly effect on the corrosion properties of steels and alloys. Therefore, this study was focused on estimation of the effect of these characteristics of different type inclusions on dissolution extend of metal matrix around these inclusions during electrolytic extraction, which may be similar to corrosion processes in pipeline steels and alloys.

Different inclusions observed in 3D on film filter and metal surface after electrolytic extraction of EP718 sample were conditionally divided into four groups depending on their composition and morphology. **Table 2** shows typical SEM images, contents of the main elements and size ranges of different types of inclusions. Since the contents of such light elements as C, N and O cannot be accurately determined by EDS, their contents did not give in the **Table 2.**

Table 2. Typical inclusions observed after electrolytic extraction of EP718 sample

Preprints (www.preprints.org) | NOT PEER-REVIEWED | Posted: 19 July 2020 doi:10.20944/preprints202007.0428.v1

Peer-reviewed version available at Metals 2020, 10, 1177; doi:10.3390/met10091177

Type	SEM image on film filter	SEM image on metal surface	Composition (mass. %)	Size (μm)
NbTi-C (inclusions and clusters)	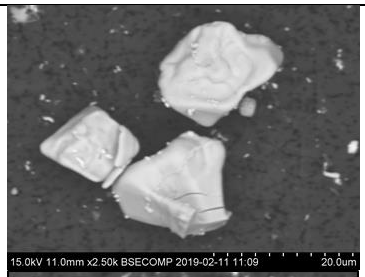	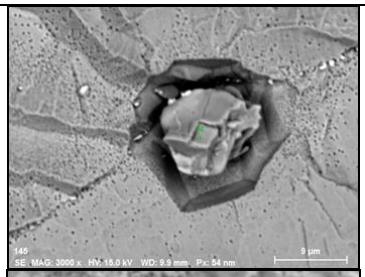	50-70% Nb, 24-45% Ti, 1-6 % W,	3-40
TiNb-N, TiNb-NC (inclusions and clusters)	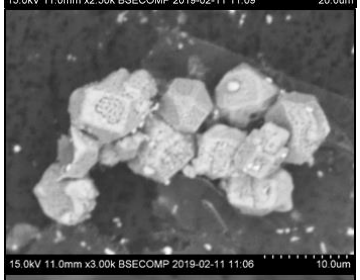		48-83% Ti 2-42% Nb 0-5% W	4-26
TiNb-S, TiNb-SC (inclusions and clusters)		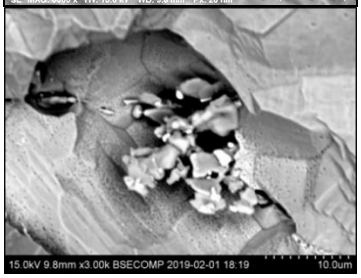	40-71% Ti, 14-33% Nb 0-4% W, 0-3% Mo 7-21% S	2-37
NbTiMoWCr-C	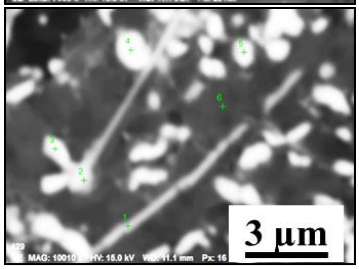	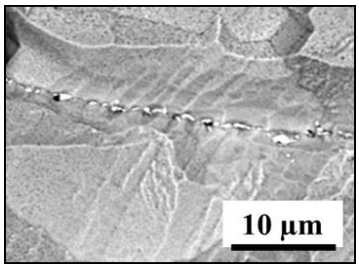	8-57% Nb, 3-42% Ti 0-38% Mo, 0-26%W 3-25% Cr	0,5-12

It was found that the sample of EP718 alloy contains the following typical inclusions:

1. Irregular or regular carbides of Nb and Ti contained also up to 1-6% of W (NbTi-C type) having sizes of 3-40 μm. A ratio of Nb and Ti contents of these carbides ($R_{Nb/Ti}$ = %Nb / %Ti) in these inclusions varied from 1.2 up to 2.4 and had an average value of 1.6±0.2.
2. Regular nitrides of Ti and Nb (TiNb-N type) contained up to 5% of W and had a size of 4-26 μm. Moreover, these inclusions contained sometimes also a small amount of carbides of these elements. The value of a $R_{Nb/Ti}$ in these nitrides was from 0.2 up to 0.6 (0.3±0.2 on average) depending on the fraction of NbTi-C inclusions precipitated on nitrides.
3. Irregular sulphides of Ti and Nb (TiNb-S type) contained 7-21% of S, ≤ 4% of W and ≤ 3% of Mo. These sulfides having size of 2-37 μm were observed mostly as clusters on grain boundaries of a metal sample along the deformation direction in combination with carbides (**Table 2**). The value of a $R_{Nb/Ti}$ in these sulfides was from 0.2 up to 0.7 (0.5±0.2 on average) depending on the fraction of carbide inclusions. Moreover, it was found that these types of sulfides, that were detected as acicular inclusions by using a conventional 2D investigations on polished surface of metal samples, have a plate or petal-like shape with thickness 1-2 μm, as can be seen in **Table 2.**
4. Small size multicomponent carbides (0.5-4 μm) contain Nb, Ti, Mo, W and Cr (NbTiMoWCr-C type) and have different morphologies (such as spherical, irregular and acicular shapes). Length of acicular inclusions can be up to 12 μm. The contents of main elements in these inclusions, may vary ($R_{Nb/Ti}$ = 1.4±0.5), as can be seen in **Table 2.** This type of inclusions was observed mostly on grain boundaries of metal matrix and partially on surfaces of different inclusions. Based on the

Peer-reviewed version available at Metals 2020, 10, 1177; doi:10.3390/met10091177

location, morphology and compositions, it can be safely assumed that these inclusions precipitated in a solidified metal matrix during cooling and heat treatment.

It should be noted that the NbTi-C and TiNb-N inclusions were observed on film filter and metal surface after electrolytic extraction as separate particles as well as clusters or group of particles located very close to each other, which summarized size is significantly larger (in most cases) than that of separate particles. Moreover, sometimes the inclusions of different types were observed together in one group or located close to each other.

Based on the composition and morphology, different inclusions observed in alloy 718 were conditionally divided into the three following groups (as shown in **):**

1. Regular and irregular carbides of Nb and Ti (NbTi-C type) contained also 0-7% of Cr and having sizes 2-30 μm. The ratio of Nb and Ti contents of these carbides (RNb/Ti) in these inclusions was varied in the wide range (from 3.4 up to 23) and has an average value of 9.9±3.7. These NbTi-C inclusions were observed on film filter and metal surface as separate particles as well as clusters or group of particles located very close to each other, as shown in .
2. Large size irregular nitrides of Ti and Nb (TiNb-N type) having size of 9-27 μm. The value of a RNb/Ti in these nitrides was from 0.2 up to 0.9 μm (0.3±0.2 on average). These nitride inclusions are usually located in metal matrix as separate particles.
3. Small size carbides (0.5-8 μm) contain mostly Nb, Ti and 1-3% Cr (NbTi-C) and can have spherical, irregular or acicular shapes, as shown in . The value of a RNb/Ti in these nitrides varied in the wide range from 5.6 up to 14.9 μm (on average 8.6±2.1). These small size carbides were located usually on grain boundaries of metal matrix and sometimes on surfaces of different inclusions, as can be seen in . It was assumed that these small carbides precipitated in a solidified metal matrix during heat treatment.

Table 3. Typical inclusions observed after electrolytic extraction of alloy 718 alloy

Type	SEM image on film filter	SEM image on metal surface	Composition (mass. %)	Size (μm)
NbTi-C (inclusions and clusters)	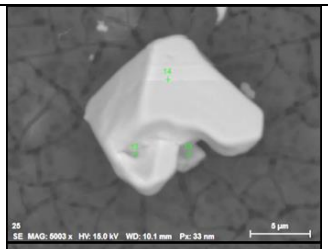	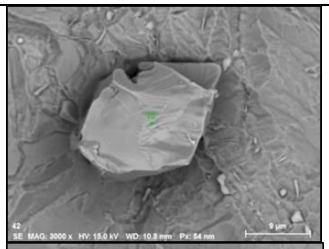	72-96% Nb, 2-16% Ti, 0-7% Cr	2-30
TiNb-N,	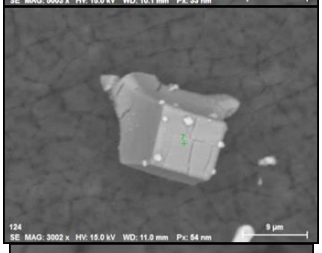	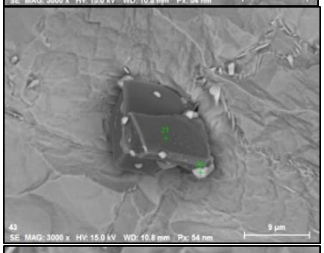	59-79% Ti, 9-39% Nb	9-27
NbTiCr-C	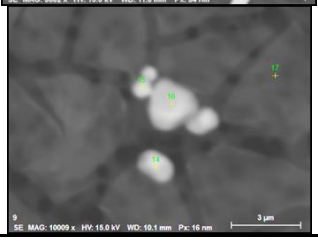	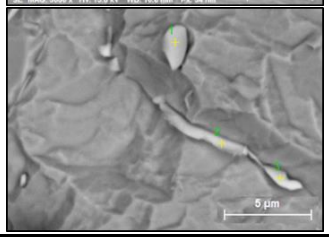	78-93% Nb, 6-15% Ti, 1-3% Cr	0.5-8

Peer-reviewed version available at Metals 2020, 10, 1177; doi:10.3390/met10091177

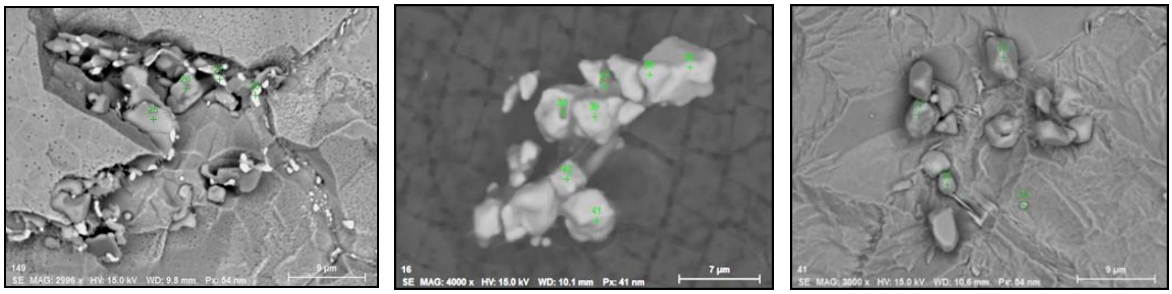

(a) **(b)** **(c)**

Figure 2. Typical SEM images of NbTi-C clusters in EP718 alloy on metal surface **(a)** and in alloy 718 on film filter **(b)** and of the group of NbTi-C inclusions located closely each other on metal surface **(c)** observed after EE

3.2. Effect of inclusions on corrosion resistance

After electrolytic extraction, the surfaces of metal samples were investigated for evaluation of characteristics and location of different inclusions in a metal matrix. It was found that the small size inclusions (such as NbTiMoWCr-C in EP718 alloy and NbTiCr-C in alloy 718) and sulfides (TiNb-S and TiNb-SC in the EP718 alloy) are located mostly on grain boundaries of metal matrix though large size nitrides and carbides in these Ni-based alloys can be observed both on grain boundaries as well inside metal grains.

Also, it was detected that the metal matrix was not evenly dissolved during the electrolytic extraction process around different inclusions. As can be seen in **Figure 3,** the dissolution of metal matrix around some inclusions was almost uniform (**Figure 3,** a) as in most areas of metal sample, whereas large size "craters" of metal dissolution was observed around other inclusions and clusters (**Figure 3,** b). Moreover, significant metal dissolution as "ditches" was observed on grain boundaries of the EP718 sample. These formed craters and ditches around some inclusions and on grain boundaries can be explained by the easier electro-chemical dissolution of the weakened metal matrix around these corrosion-active inclusions and on grain boundaries during electrolytic extraction. However, according to publications of Inoue et al. [13], the 10%AA electrolyte used in this study for electrolytic extraction does not dissolve the inclusions observed in these alloy samples. In other words, these inclusions are not involved directly in dissolution process of the metal matrix around these inclusions due to some additional electro-chemical reactions. As a result, it can allow us to assess the corrosion resistance of metal matrix around different inclusions and to detect the inclusions having most harmful effect on weakened of metal matrix around these inclusions.

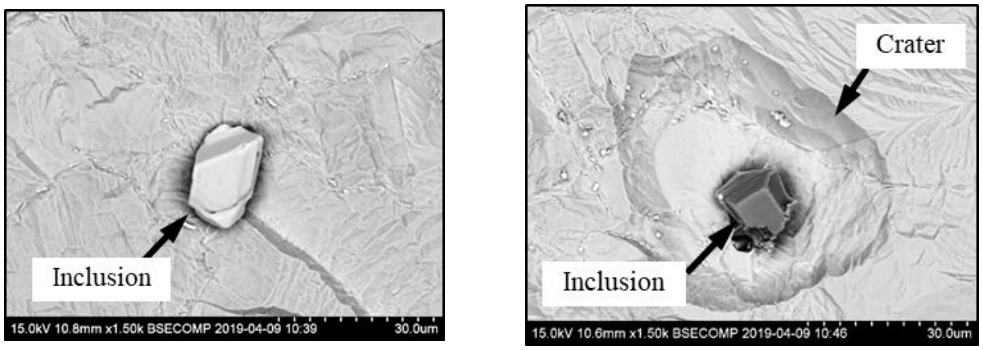

(a) **(b)**

Peer-reviewed version available at Metals 2020, 10, 1177; doi:10.3390/met10091177

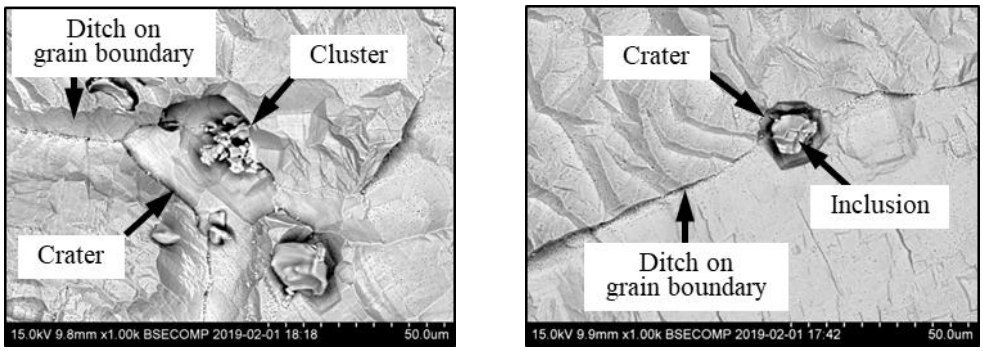

(c) **(d)**

Figure 3. Typical SEM images of metal dissolution around different inclusions and clusters observed on the surface of metal sample after electrolytic extraction. (a), uniform dissolution around inclusion, (b) dissolution inclusions on grain boundaries, (c)dissolution around craters, (d) craters around inclusion

In order to clarify the degree of influence of various inclusions on the corrosion resistance, the dissolution of the matrix near the inclusions on the surface of the metal samples was analyzed after electrolytic extraction. The extent of metal matrix dissolution around various inclusions after electrolytic extraction was estimated and compared by determination of the diameter of the dissolution crater around inclusions (D_{cr}, Equation 1) and relative coefficient of metal dissolution (KD, Equation 2). Comparison of some characteristics of different inclusions, size ranges of craters (D_{cr}) and average KD values (including value of standard deviation) in investigated alloy samples are given in **Table 4.**

Table 4. Characteristics of different inclusions and dissolution of metal matrix around inclusions obtained for different alloy samples

Alloy	Type of inclusion	Average $R_{Nb/Ti}$ (= %Nb / %Ti)	Size range of inclusions (µm)	Size of crater, *Dcr* (µm)	Average *KD*
EP718	NbTi-C	1.6 ± 0.2	3 - 40	6 - 24 (16 - 40) *	2.4 ± 1.1 (4.9 ± 3.7) *
	TiNb-N	0.3 ± 0.2	4 - 26	9 - 10 (-)	2.8 ± 0.9 (-)
	TiNb-S	0.3 ± 0.2	2 - 37 (-)	- (15 - 40)	- (8.8 ± 3.6)
	NbTiMoWCr-C	1.4 ± 0.5	0,5 - 12	- (8 - 12)	- (21.3 ± 7.7)
Alloy 718	NbTi-C	9.9 ± 3.7	2 - 30	6 - 21 (11 - 40)	2.2 ± 0.8 (5.1 ± 2.7)
	TiNb-N	0.3 ± 0.2	9 - 27	17 - 26 (24 - 36)	2.4 ± 0.1 (6.5 ± 5.5)

Peer-reviewed version available at Metals 2020, 10, 1177; doi:10.3390/met10091177

NbTiCr-C	8.6 ± 2.1	0.5 - 8	- (2 - 7)	- (5.2 ± 3.2)

* - Values for inclusions located at grain boundaries are indicated in parentheses.

Based on the obtained results, relationships between sizes of different inclusions, their locations in metal matrix and dissolution parameters (*KD* and D_{cr}) are shown in **Figure 4** and**Figure 4 Figure 4Figure 5** for EP718 alloy and alloy 718, res

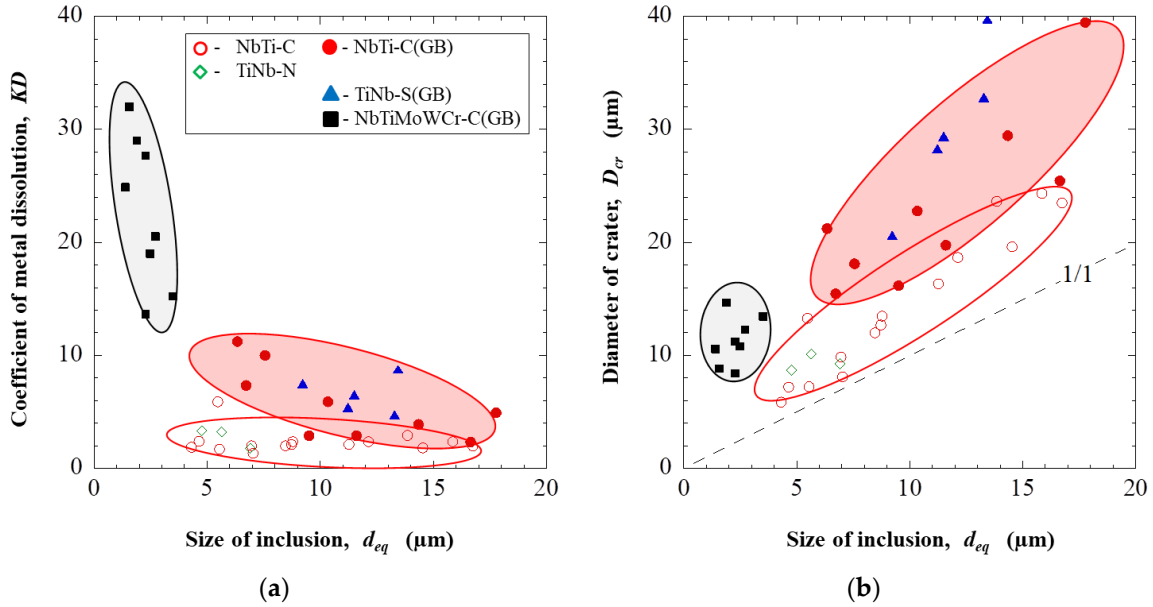

Figure 4. Effect of the composition, size and location of inclusions in the EP718 alloy on the dissolution coefficient **(a)** and diameter of crater around inclusions **(b)**

According to the obtained results given in **Table 4** and **Figure 4**, the largest size of craters (D_{cr} up to 40 µm) has the NbTi-C and TiNb-S inclusions of titanium carbides, niobium, and titanium sulfides located along grain boundaries in EP718 sample. The average dissolution coefficients of metal matrix around these inclusions (*KD*) are 4.9 and 8.8, respectively, which suggests that sulfides are more active in terms of corrosion. Titanium sulfides, which are rarely mentioned in the literature, were also detected in the EP718 alloy. Nevertheless, it is known that sulfides are corrosive inclusions that significantly reduce pitting resistance (from 3 to 100 times) and are preferred centers for pitting, especially in chloride environments [5, 9, 35].

It should be pointed out that the NbTi-C inclusions located inside of grains have 2 times smaller values of D_{cr} and *KD* compared to those for inclusions located on grain boundaries. Moreover, it can be seen that the small amount of NbTiMoWCr-C inclusions located at the grain boundaries have the highest values of dissolution coefficient KD (from 14 up to 32) compared to the other types of inclusions. It can be explained by the depletion of the metal matrix around of these inclusions by the alloying elements (such as chromium, molybdenum and tungsten), which are contained in these inclusions and responsible for corrosion resistance of metal matrix. However, the size of the craters/ditches around these inclusions is relatively small (less than 15 µm) compared with other types of inclusions due to their smaller size.

The TiNb-N inclusions were observed inside the grains and, judging by the low dissolution coefficient (KD~2.8) and small diameter of craters (9-10 µm), have a lower effect on corrosion, which confirms literature data [21].

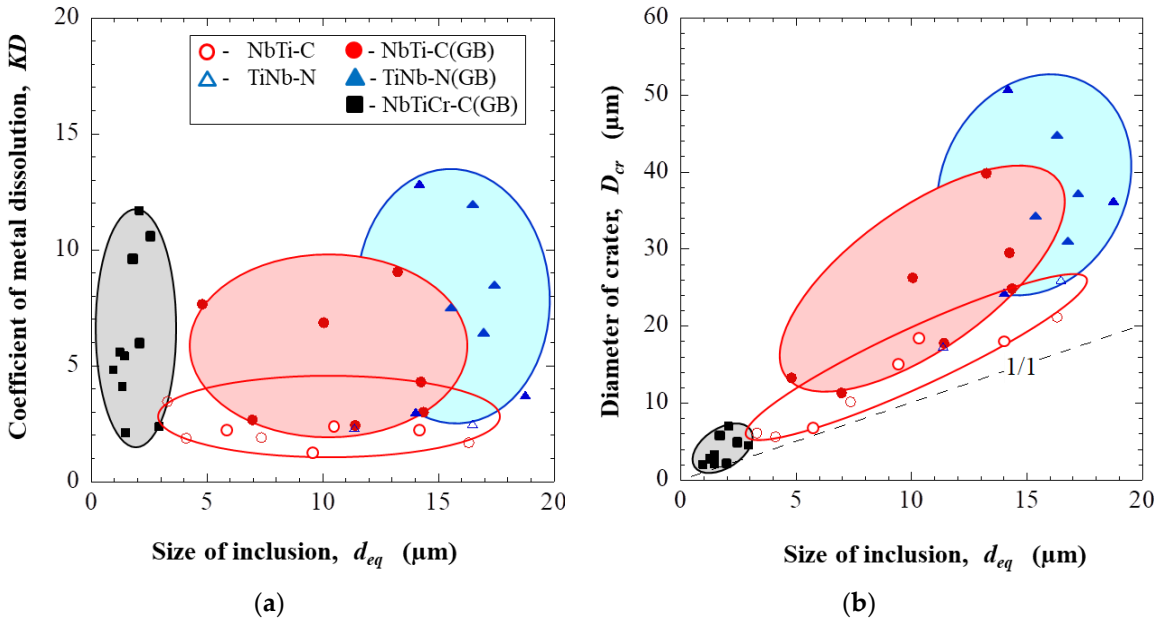

Figure 5. Effect of the composition, size and location of inclusions in the alloy 718 on the dissolution coefficient **(a)** and diameter of crater around inclusions **(b)**

As it can be seen in **Table 4** and **Figure 5**, the largest craters in the alloy 718 were observed around TiNb-N (D_{cr} = 24-51 µm) and NbTi-C (D_{cr} = 16-40 µm) inclusions located at the grain boundaries. At that the size of craters around these types of inclusions tends to increase significantly with an increasing of equivalent size (D_{eq}) of inclusions. Though the *KD* coefficient for these inclusions can be varied in a wide range (from 2 up to 13), the dissolution coefficient of metal matrix around these inclusions located on grain boundaries is on average 2.5 times larger compared to those located inside of grains.

The values of *KD* for small size NbTiCr-C inclusions, which are located mostly on grain boundaries, can be varied in a wide range (from 2 up to 12) although the size of craters/ditches around these inclusions in this 718 alloy usually is much smaller (D_{cr} = 2-7 µm) compared to that of other types of inclusions. It is interesting to point out that these NbTiCr-C inclusions, which also contained chromium as a corrosion resistance alloying element, did not show practically any particular effect on corrosion dissolution of metal matrix in the 718 alloy. It may be explained by much lower content of Cr (1-3%) in these small carbides in the 718 alloy compared to the contents of alloying elements (3-25% Cr, 0-38% Mo and 0-26% W) in NbTiMoWCr-C inclusions in EP718 alloy. Therefore, the metal matrix around these small NbTiCr-C inclusions has no (or has too small) concentration depletion by the alloying elements (such as Cr). As a result, the dissolution of metal matrix (*KD*) around these small inclusions on grain boundaries in the 718 alloy is much smaller (~4 times) compared to that in the EP718 alloy.

4. Discussion

Based on comparative analysis of inclusions and dissolution of metal matrix around these inclusions after electrolytic extraction of EP718 and 718 alloys, the inclusions harmful for corrosion properties of alloys were determined.

Similar types of inclusions (such as NbTi-C and TiNb-N) which correspond primary MC carbides based on the chemistry and morphology and are formed when solidifying [33, 34] were found in both Ni-based alloys, For both studied nickel based alloys, the dissolution of metal matrix around of NbTi-C inclusions and clusters have very similar dissolution parameters as for inclusions located inside the grains as well for inclusions located on grain boundaries, as it can be seen in Table 4. However, it should be pointed out that these carbides in the 718 alloy contain a much larger amount of Nb ($R_{Nb/Ti}$ = 9.9±3.7) compared to that in the EP718 alloy (RNb/Ti = 1.6±0.2), which can be explained by the larger content of Nb in the alloy 718 (up to 5.2%).

Peer-reviewed version available at Metals 2020, 10, 1177; doi:10.3390/met10091177

It was found that compositions of TiNb-N inclusions that are MN nitrides with formed even with insignificant amount of nitrogen in both samples are very similar (RNb/Ti = 0.3±0.2) [33, 34]. However, despite the fact that the average dissolution coefficients (KD) for nitrides (TiNb-N) in both alloys are similar (2.8 in EP718 alloy and 2.4 in alloy 718), the equivalent diameter of "craters" in alloy 718 is significantly larger (*Dcr* = 17-26 μm) compared to that in EP718 alloy (Dcr = 9-10 μm). It can be explained by a larger amount of nitrides observed in the alloy 718 samples, though some number of large sized nitride clusters was also found in the EP718 sample. Moreover, most of the large size TiNb-N inclusions in the 718 alloy are located on grain boundaries of metal matrix, for which dissolution parameters are much higher (KD = 6.5±5.5 and Dcr = 24-36 μm). Thus, despite the fact that nitrides are considered the most neutral from the point of view of corrosion, but with their large sizes (10-27 μm), they can harmfully effect the corrosion resistance by increasing the area of the cathode.

Both alloys are also characterized by a more active harmful effect of all types of inclusions located along grain boundaries. The values of the dissolution coefficient *KD* for inclusions located at grain boundaries are from 2.1 to 2.7 times larger than that for inclusions located in the grain for both investigated alloys. The dissolution coefficient of metal matrix around TiNb-S inclusions and clusters (*KD* = 8.8±3.6), which were found on grain boundaries in the EP718 alloy, is considerably larger compared to that for NbTi-C and TiNb-N inclusions in this alloy. Therefore, this type of sulphides should be considered as very harmful inclusions, which can significantly increase a pitting corrosion of the EP718 alloy.

The dissolution coefficient for small chromium-containing carbide inclusions located on grain boundaries is much lower for alloy 718 (*KD* = 5.2±3.2) compared to that for EP718 alloy (*KD* = 21.3±7.7). In contrast to the EP718 alloy, the *KD* value for these small Cr-containing inclusions is relatively low and comparable with the dissolution coefficients for other inclusions observed in the alloy 718. This difference in behavior can be explained by the lower contents of Cr (1-3%) small carbides in 718 alloy and by the more complex composition of these carbide inclusions of the EP718 alloy (**Table 2**) contained 3-25% of Cr, 0-38% of Mo and 0-26% of W, that are M_6C carbides according to chemical composition that are formed in the temperature range 850 до 1100°C [33, 34], which are responsible for pitting resistance.

Based on the revealed differences in the composition and amount of inclusions in EP718 and 718 alloys, it can be concluded what inclusions reduce the corrosion resistance of EP718 alloy.

4. Titanium sulfides have the most negative effect on matrix dissolution;
5. Carbides, especially at the boundaries, containing chromium, molybdenum and tungsten in their composition cause a significant dissolution of the matrix around the inclusions,
6. Large (more than 10 μm) carbides and nitrides of titanium and niobium are also able to reduce corrosion resistance.

Thus, an application of the electrolytic extraction in combination with 3D investigations of different inclusions and clusters and an evaluation of electrolytic dissolution of metal matrix around these inclusions in the EP718 and 718 alloys allowed detect more harmful inclusions regarding corrosion of metal matrix in these Ni-based alloys. As a next step of the future study, the reasons of formations and mechanisms of effects of harmful inclusions on different stages of the Ni-based alloy production can be considered.

5. Conclusions

In this study, main characteristics of different inclusions (such as composition, morphology, size, number and location) and dissolution of metal matrix around these inclusions were investigated on film filter and on the surfaces of metal samples after electrolytic extraction (EE) of two industrial Ni-based alloys (alloy 718 and EP718). The obtained results can be summarized as follows:

1. The electrolytic extraction technique can be successfully applied for three-dimensional (3D) investigations of different inclusions on film filter and on the surface of metal samples after extraction of Ni-based alloys. It was shown that the morphology of inclusions is much more

complicated than can be seen on a flat section. For instance, a thin plate-like sulphides of Ti and Nb (with a thickness of 1-2 μm) were detected in clusters (up to 37 μm) are located mostly on grain boundaries in the EP718 alloy, which were detected only as separate acicular sulfides by conventional two-dimensional (2D) investigations on polished surface of this metal sample.

2. Evaluation of different extent of dissolution of metal matrix around different inclusions after EE by determination of equivalent diameter of "crater" (D_{cr}) and relative coefficient of metal matrix dissolution (*KD*) allows estimate a metal weakening around investigated inclusions, which correlates to a corrosion resistance of metal.
3. In the EP718 alloy, 4 types of inclusions were found, which are ordered according to a higher degree of influence on corrosion resistance of the alloy: TiNb-S sulfides, NbTi-C carbides, small size multicomponent carbides (NbTiMoWCr-C) and TiNb-N nitrides. Three types of typical inclusions were found in alloy 718: NbTi-C carbides, TiNb-N nitrides and small size carbides (NbTiCr-C). In addition to separate inclusions, clusters (up to 40 μm) consisting of different inclusions were found in both alloys.
4. Harmful effect of inclusions on dissolution of metal matrix decreases from the sulfides (TiNb-S) and small carbides (NbTiMoWCr-C) located on grain boundaries to the large carbides (NbTi-C) and nitrides (TiNb-N) located as on grain boundaries as well inside of grains. The nitride inclusions (TiNb-N) having the size larger than 10 μm can also significantly reduce the corrosion resistance of Ni-based alloys, although in the literature they are described as the most neutral with respect to the matrix.
5. In addition to the composition of the inclusion, their location (at the boundary or in the grain) and size also affect the corrosion resistance and the propensity to pitting. For instance, the dissolution parameters (*KD* and D_{cr}) for inclusions located on grain boundaries are from 2.1 to 2.7 times larger than that for inclusions located inside the grains for both investigated alloys. The inclusions affect differently: the composition, size, position that inclusions located at the grain boundaries are more significant reduce corrosion resistance. Large inclusions of more than 10 μm affect the corrosion resistance more significantly.

Author Contributions: Conceptualization, methodology, investigation, draft writing – A. Karasev, E. Alekseeva; resources, validation, supervision, review and editing – P. Jonsson, A. Alkhimenko; All authors have read and agreed to the published version of the manuscript.

Conflicts of Interest: The authors declare no conflict of interest.

References

1. Kazakov, A.A. Nonmetallic Inclusions in Steel – Origin, Estimation, Interpretation and Control. Proceedings of M&M conference, Columbus, USA, July 24-28 **2016**; DOI:10.1017/S1431927616010539.
2. Park, J. H.; Youngjo K. Inclusions in Stainless Steels − A Review. Steel Research International **2017**. 88 №1700130. DOI:10.1002/srin.201700130.
3. Jönsson, P.; Karasev, A.; Ånmark, N. The Influence of Microstructure and Non-Metallic Inclusions on the Machinability of Clean Steels, Materials Steel Research International **2016**, Volume 8(2), pp. 751-783, DOI: 10.1002/srin.201600111.
4. Amezhnov, A.V.; Rodionova, I.G.; Zaitsev, A.I.; Mogutnov, B.M.; Baklanova, O.N. Influence of the chemical composition of non-metallic inclusions on corrosion resistance of carbon and low-alloy steels in aqueous media typical for service conditions of oil-field pipelines. Problems of ferrous metallurgy and materials science **2018**, Volume 3, pp. 81-90.
5. Cyril, N.; Fatemi, A.; Cryderman, B. Effects of sulfur level and anisotropy of sulfide inclusions on tensile, impact, and fatigue properties of SAE 4140 steel. SAE Int. J. Manuf. Mater. **2008**, 1, pp. 218–227.
6. Kazakov, A.; Zhitenev, A.; Kovalev, P. Distribution Pattern of Nonmetallic Inclusions on a Cross Section of Continuous-Cast Steel Billets For Rails. Microsc. Microanal 2015, Volume 21 (Suppl. 3), Paper No. 0874, pp.1751-1752, DOI:10.1017/S1431927615009538.

7. Bettini, E.; Kivisäkk, U.; Leygraf, C.; Pan, J. Study of corrosion behavior of a 22% Cr duplex stainless steel: influence of nano-sized chromium nitrides and exposure temperature. Electrochim. Acta **2013**, Volume 113, pp. 280–289.
8. Knyazeva, M.; Pohl, M.; Duplex Steels. Part II: Carbides and Nitrides Metallogr. Microstruct. Anal. **2013**, Volume 2, pp.343–351, DOI 10.1007/s13632-013-0088-2.
9. Muto, I.; Ito, D.; Hara, N. Microelectrochemical Investigation on Pit Initiation at Sulfide and Oxide Inclusions in Type 304 Stainless Steel. Journal of The Electrochemical Society **2009**, Volume 156, Number 2, DOI:10.1149/1.3033498.
10. Shakhmatov, A.V.; Badrak, R.P.; Kolesov, S.S.; Kharkov, A.A. Influence of structure on the corrosion properties of high manganese high nitrogen stainless steels, Proceedings of European Corrosion Congress **2015**, (EUROCORR' 2015), Graz, Austria, 6 -10 September 2015.
11. Matsuura, H.; Choi, W.; Kamimura, G. Evolution of Non-metallic Inclusions in Solid Fe–Al–Ti–N Alloy During Heating. In: Hwang JY. et al. (eds) 8th International Symposium on High-Temperature Metallurgical Processing. The Minerals, Metals & Materials Series. Springer, Cham, 2017.
12. Urbano, M. F.; Coda, A. Beretta, S. Cadelli A., and Sczerzenie, F. The Effect of Inclusions on Fatigue Properties for Nitinol, in Fatigue and Fracture Metallic Medical Materials and Devices, ed. M. Mitchell, S. Smith, T. Woods, and B. Berg, West Conshohocken, ASTM International **2013,** pp. 18-34. https://doi.org/10.1520/STP155920120189
13. Prillhofer, B.; Antrekowitsch H.; Böttcher, H.; Enright, P. Nonmetallic inclusions in the secondary aluminium industry for the production of aerospace alloys, TMS light metal conference, Oxfordshire, England , 2008.
14. Xu, J.; John, H.; Wiese, G.; Liu X. Oil-grade alloy 718 in oil field drilling application. Proceedings of 7th International Symposium on Superalloy 718 and Derivatives TMS (The Minerals, Metals & Materials Society), October 10-13 Pittsburgh, USA, 2010, pp. 923-932.
15. Ramirez, E.; Garfias-Mesias, L. In-situ Studies of Precursor Sites for Pit Initiation on Corrosion Resistant Alloys in Chloride Containing Solutions, NACE Corrosion conference proceedings, Houston, USA, 2013, paper № 2428.
16. Lackner, R.; Mori, G.; Prohaska, M.; Egger, R.; Tichler, G.; UNS 06626: precipitation and sensitization. Proceeding of NACE Corrosion conference 2013, Houston, USA, March 7-12, pp. 24-40.
17. OBASI, G.C.; ZHANG, Z.; SAMPATH, D.; MORANA, R.; AKID, R.; PREUSS. M. Effect of Microstructure and Alloy Chemistry on Hydrogen Embrittlement of Precipitation-Hardened Ni-Based Alloys, Metallurgical And Materials Transactions (A) **2018**, Volume 49A, pp. 1167-1181, https://doi.org/10.1007/s11661-018-4483-9.
18. Pahlavanyali, S.; Wood, M.; Marchant, G. The Effect Of Carbide Decomposition And Reformation on Rupture Lives of In738lc During Multiple Reheat Treatment And Degradation Cycles, Proceedings of TMS conference, Orlando, USA, March 11-15 2012, pp.463-471.
19. Tormoen, G.; Sridhar, N.; Anderko, A. Localized corrosion of heat treated alloys part 1 – repassivation potential of alloy 600 as function of solution chemistry and thermal aging. Corrosion engineering. Sci Technol. **2010**, Volume 45(2), pp.155–162.
20. Garfias-Mesias, F.; Klapper,. H.; Klower, J. Determination of Precursor Sites for Pitting Corrosion of UNS N07718 in Chloride Environments - Part 2, Proceeding of NACE Corrosion conference 2018, Phoenix, USA, April 15-19, pp. 51318-11387.
21. Klöwer, J.; Tarzimoghadam, Z.; Gosheva, O.; Klapper, H.S. Effect of Microstructural Particularities on the Corrosion Resistance of Nickel Alloy UNS N07718 – What Really Makes the Difference? Proceeding of NACE Corrosion conference 2017, New Orleans, USA, March 26 – 30, 2017, paper № 9068.
22. Klapper, H.S.; Zadorozne, N.S.; Rebak, R.B. Localized corrosion of nickel alloys: review, Acta Metall.Sinica **2017**, Vol.30, №4, pp. 296-305.
23. Mishra, A.; Richesin, D.; Rebak, R.B. Localized corrosion study of Ni-Cr-Mo alloys for oil and gas applications, Proceeding of NACE - International Corrosion Conference Series 2015, Dallas, USA, 15-19 March 2015, paper № 5802.
24. Khar'kov, A. A.; Shakhmatov, A. V.; Gyulikhandanov, E. L.; Alekseeva, E.L. Comparative Analysis of Corrosion-Resistant Alloys Inconel 718 and ÉP718. Chemical and Petroleum Engineering **2019**, V. 54, № 9–10, pp. 771–778. DOI: 10.1007/s10556-019-00546-4.

25. Gyulikhandanov E. L., Alekseeva E. L., Shakhmatov A. V., Loshachenko A. S., Lapechenkov A. A. Structure and properties of nickel-based alloy EP718 in the process of manufacturing. Voprosy Materialovedeniya (in Russian) **2019**, № 4 (100), pp. 42-52. DOI:10.22349/1994-6716-2019-100-4-42-52
26. Aghajani, A.; Alireza, J.; Parsa, B.; Kloewer, J. Identification of Mo-Rich M23C6 carbides in Alloy 718. Metallurgical and Materials Transactions **2016**, 47A (9), pp. 4382–4392.
27. Golenishcheva, O.; Klöwer, J.; Aghajani, A.; Oechsner, M.; Andersohn, G. Influence of Delta-phase Precipitation on the Pitting Performance of UNS N07718. NACE Corrosion conference proceedings 2014, Houston, USA, March 2014, paper № 3895.
28. Saleem, B.; Dong, H. Phase Characterization of CRA Fastener INCONEL718 in Relation of Hydrogen Assisted Cracking. Proceedings of Materials Today: 2S 2015, pp. 383 – 392. DOI: 10.1016/j.matpr.2015.05.053.
29. Liu, L. Effects of precipitation phases on the hydrogen embrittlement sensitivity of Inconel 718. Science and Technology of Advanced Materials 3 **2002**, pp. 335-344.
30. Badrak, R.; Howie, W.; Delacruz, A.; Kolesov, S. Characterization of direct metal laser sintered alloy 718 in the as-fabricated and heat treated condition, Proceedings of NACE - International Corrosion 2018 conference, Phoenix, USA, April 15-19, paper № 11297.
31. Labre, C.; Pinto, A.L.; Solórzano, I.G. Microstructure Evolution of Ni-base Superalloy 625: from Conventional Thermomechanical Processed to Selective Laser Melting Processed, Microsc. Microanal **2017**, 23 (Suppl. 1), pp 2250-2251, doi:10.1017/S1431927617011916.
32. Inoue R.; Kiyokawa K.; Tomoda K.; Ueda Sh.; Ariyama T. Three-Dimensional Estimation of Multi-Component Inclusion Particle in Steel, Proceedings of the 8th International Workshop on Progress in Analytical Chemistry and Materials Characterisation in the Steel and Metal Industries, CETAS-2011, Luxembourg, May 17-19, 2011, OC17, pp. 118-125.
33. T. Sims, N. S. Stoloff and W. C. Hagel, Superalloys II, John Wiley & Sons: New York, USA, 1987. P.640.
34. ASM Specialty Handbook, Nickel, Cobalt and Their Alloys, ASM Inter,. USA, 2000; pp. 442
35. Wijesinghe, T. S. L.; Blackwood, D. J., Real time pit initiation studies on stainless steels: the effect of sulphide inclusions. Corrosion Science **2007**, 49 (4), pp.1755- 1764. https://doi.org/10.1016/j.corsci.2006.10.025.